Air-mass Origin in the Arctic. Part II: Response to Increases in Greenhouse Gases

CLARA ORBE,* PAUL A. NEWMAN,* DARRYN W. WAUGH,+ MARK HOLZER,#,@ LUKE D. OMAN,* FENG LI,& AND LORENZO M. POLVANI@,**

* *Laboratory for Atmospheric Chemistry and Dynamics, NASA Goddard Space Flight Center, Greenbelt, Maryland*
+ *Department of Earth and Planetary Sciences, Johns Hopkins University, Baltimore, Maryland*
# *Department of Applied Mathematics, School of Mathematics and Statistics, University of New South Wales, Sydney, New South Wales, Australia*
@ *Department of Applied Physics and Applied Mathematics, Columbia University, New York, New York*
& *Goddard Earth Sciences Technology and Research, Universities Space Research Association, Columbia, Maryland*
** *Lamont-Doherty Earth Observatory, Columbia University, Palisades, New York*

(Manuscript received 23 April 2015, in final form 16 July 2015)

ABSTRACT

Future changes in transport from Northern Hemisphere (NH) midlatitudes into the Arctic are examined using rigorously defined air-mass fractions that partition air in the Arctic according to where it last had contact with the planetary boundary layer (PBL). Boreal winter (December–February) and summer (June–August) air-mass fraction climatologies are calculated for the modeled climate of the Goddard Earth Observing System Chemistry–Climate Model (GEOSCCM) forced with the end-of-twenty-first century greenhouse gases and ozone-depleting substances. The modeled projections indicate that the fraction of air in the Arctic that last contacted the PBL over NH midlatitudes (or air of ''midlatitude origin'') will increase by about 10% in both winter and summer. The projected increases during winter are largest in the upper and middle Arctic troposphere, where they reflect an upward and poleward shift in the transient eddy meridional wind, a robust dynamical response among comprehensive climate models. The boreal winter response is dominated by (~5%–10%) increases in the air-mass fractions originating over the eastern Pacific and the Atlantic, while the response in boreal summer mainly reflects (~5%) increases in air of Asian and North American origin. The results herein suggest that future changes in transport from midlatitudes may impact the composition—and, hence, radiative budget—in the Arctic, independent of changes in emissions.

1. Introduction

There is mounting observational evidence of drastic climate change in the Arctic, ranging from considerable sea ice loss (e.g., Rothrock et al. 1999; Wadhams and Davis 2000; Comiso 2002; Serreze et al. 2003) to rapid surface warming (e.g., ACIA 2004; Serreze and Francis 2006; IPCC 2013). Still more changes are expected to occur in future decades, with comprehensive climate models projecting that Arctic surface air temperatures will warm by about 5°C by the end of the twenty-first century—faster than any other region on Earth (IPCC 2013)—and that there will be a complete disappearance of summer Arctic sea ice by midcentury (Holland et al. 2006).

While climate change in the Arctic is driven largely by increases in long-lived greenhouse gases (GHGs), increases in shorter-lived trace species and aerosols have also accelerated warming by altering the radiative and chemical properties of the Arctic. For example, in recent decades increased black carbon deposition on snow and ice has significantly enhanced surface longwave fluxes over the Arctic and may have been twice as effective as carbon dioxide at warming the Arctic surface (Koch and Hansen 2005). Simulations with comprehensive climate models also indicate that increased levels of ozone precursors, including nitrogen oxides and volatile organic compounds, have contributed as much as 30% to the observed positive trends in twentieth-century Arctic surface temperatures by increasing high-latitude tropospheric ozone (Shindell et al. 2006). Therefore, a comprehensive understanding of the current and future

Corresponding author address: Clara Orbe, Laboratory for Atmospheric Chemistry and Dynamics, NASA Goddard Space Flight Center, Greenbelt, MD 20771.
E-mail: clara.orbe@nasa.gov

DOI: 10.1175/JCLI-D-15-0296.1

distributions of chemical and particulate tracers in the Arctic is key for understanding climate.

It is now well appreciated that nearly all of the pollution in the Arctic originates over Northern Hemisphere (NH) midlatitudes (Law and Stohl 2007). Since the distributions of trace species reflect the full interplay between emissions, chemistry, and transport, Arctic pollution in the future will reflect not only changes in species' emissions and chemistry, but also changes in the large-scale circulation. However, while the climate-change signature on large-scale dynamics has been examined in both models and observations [e.g., shifts in the midlatitude tropospheric jets (e.g., Yin 2005; Miller et al. 2006; Barnes and Polvani 2013), the expansion and weakening of the Hadley cell (e.g., Lu et al. 2007), and trends in atmospheric variability (e.g., Hurrell 1995; Thompson et al. 2000; Zhou et al. 2001)], relatively little attention has been paid to assessing the large-scale response of transport into the Arctic.

Here we quantify tropospheric transport using idealized tracers that partition the air in the Arctic according to the regions where it last contacted the planetary boundary layer (PBL). In Orbe et al. (2015, hereinafter Part I), we presented the first model climatology of Arctic air-mass origin in terms of rigorously defined air-mass fractions $f(\mathbf{r} \mid \Omega_i)$ that quantify the fraction of air at location $\mathbf{r}$ that last contacted the PBL over the origin region Ω_i. (Note that the term ''origin'' is used in reference to the region where air last contacted the PBL.) In practice $f(\mathbf{r} \mid \Omega_i)$ is calculated as a simple equilibrated tracer mixing ratio that shows where in the Arctic, and with what dilution, the air from an origin region can be found.

Air-mass origin climatologies for NH winter [December–February (DJF)] and NH summer [June–August (JJA)] were presented in Part I based on calculations from a time-slice integration of the Goddard Earth Observing System Chemistry–Climate Model (GEOSCCM) subject to forcings representative of the present-day climate [i.e., fixed 2010–19 time-averaged GHGs and ozone-depleting substances (ODS)]. It was shown that the Arctic middle and upper troposphere (i.e., above 700 hPa) consists largely of air that last contacted the PBL over latitudes between 25° and 60°N, defined herein as NH midlatitudes. Last contact at the midlatitude PBL occurs primarily over the oceans during NH winter and over land during NH summer, consistent with ventilation of the midlatitude boundary layer by the storm tracks and large-scale convection, respectively. It was also shown that during NH winter last contact at the midlatitude surface occurs primarily over the eastern Pacific, where strong poleward flow ensures that air is efficiently transported to the Arctic with little chance of reencountering the PBL. By comparison, during summer air of NH midlatitude origin last contacts the PBL primarily over Asia, consistent with strong convection and mean poleward flow over Siberia.

In Part I different features of the large-scale circulation were used to interpret the seasonal cycle of air-mass origin in the Arctic and its partitioning with respect to the different PBL regions. Here we ask how future changes in the midlatitude storm tracks, large-scale stationary waves, and large-scale vertical motions over NH midlatitudes will affect transport into the Arctic in terms of the regions where air last contacts the PBL. In particular, recent studies have shown that, while comprehensive climate models project that the zonal-mean midlatitude tropospheric jet will shift poleward by the end of the twenty-first century, the longitudinally varying response is highly variable across basins and between seasons, at places featuring robust equatorward shifts (Barnes and Polvani 2013; Simpson et al. 2014). And yet, while strong longitudinal variations in the jet response may have large impacts on regional transport and climate (Simpson et al. 2014), these transport changes have yet to be assessed.

In addition to future changes in the tropospheric midlatitude jet, comprehensive models also indicate that dry static stability over midlatitudes will increase in response to GHG-induced warming, with the largest increases occurring during NH summer (Wetherald and Manabe 1988; Frierson 2006). Although increases in tropospheric stability have been linked to the projected weakening and delayed onset of the North American monsoon in a warmer climate (Cook and Seager 2013), a systematic examination of the corresponding transport response in the Arctic has not been performed.

Here we examine how transport into the Arctic will change by the end of the twenty-first century by examining differences in the climatological air-mass fractions between two time-slice integrations of GEOSCCM: the present-day or reference (REF) integration presented in Part I and a future (FTR) integration forced with greenhouse gases and ozone-depleting substances representative of the end of the twenty-first century. After briefly describing the model and simulation in section 2, we present the model's dynamical large-scale response to changes in greenhouse gases in section 3 and the projected changes in the air-mass fractions in section 4, followed by conclusions in section 5.

2. Model simulation and diagnostic tracers

Air-mass fractions for the future climate are calculated using a 20-yr-long time-slice integration of GEOSCCM

subject to 2080–2100 time-averaged greenhouse gases and ozone-depleting substances under the SRES A1B and A1 scenarios respectively. As for the present-day integration presented in Part I, which was also integrated for 20 model years, sea surface temperatures and sea ice concentrations are taken from an integration of the NCAR Community Climate System Model, version 3.0, subject to A1B GHG forcing, except that time averages have now been taken over the model years 2080–2100. For more details about the model we refer the reader to section 2 in Part I.

For both the REF and FTR integrations, air-mass origin regions are defined with respect to the model's PBL, which is first partitioned into three zonally symmetric origin regions: a "southern latitude patch" ($\Omega_{\rm STH}$) spanning latitudes south of 25°N, a "midlatitude patch" ($\Omega_{\rm MID}$) between 25° and 60°N, and an "Arctic patch" poleward of 60°N ($\Omega_{\rm ARC}$; Fig. 1 in Part I). In addition, six nonoverlapping origin regions within $\Omega_{\rm MID}$ are defined over the eastern Pacific, North America, the Atlantic, Europe, Asia, and the western Pacific, denoted throughout using the labels EPAC, NAM, ATL, EUR, ASI, and WPAC, respectively.

Following spinup of the dynamical variables, nine tracers, corresponding to the nine Ω_i origin regions, are integrated for 20 years for the future (FTR) integration. Once air masses have reached equilibrium, their annual (ANN), wintertime (DJF), and summertime (JJA) climatological mean fractions are calculated over the last 10 years of the integration, and are denoted as $\overline{f}^{\rm ANN}(\mathbf{r}\,|\,\Omega_i)$, $\overline{f}^{\rm DJF}(\mathbf{r}\,|\,\Omega_i)$, and $\overline{f}^{\rm JJA}(\mathbf{r}\,|\,\Omega_i)$, where the overbar denotes time averaging over the respective time period. Furthermore, for consistency with Part I, the air-mass fraction corresponding to the region Ω_i is referred to throughout as "Ω_i air". For example, $\Omega_{\rm STH}$ air (also "southern air" or "air of southern origin") refers to the air-mass fraction at $\mathbf{r}$ that last encountered the PBL south of 25°N.

Climate changes in the air-mass fractions are expressed in terms of the differences between the FTR and REF 10-yr averaged climatologies and denoted throughout using the notation $\Delta f(\mathbf{r}\,|\,\Omega_i)$ (where $\Delta \equiv$ FTR − REF). Note that throughout we refer to the FTR − REF changes as the responses to "increases in greenhouse gases" since the circulation changes at NH high latitudes incurred only by changes in ozone-depleting substances are relatively weaker. Statistical significance of the diagnosed climate changes in the air-mass fractions and the dynamical variables is assessed based on an independent two-sample Student's t test using the local standard deviation at each grid point $\sigma_x \equiv [N^{-1}\sum_{n=1}^{N}(\tilde{x}_n - \overline{x})^2]^{1/2}$, where $N = 10$ and $\tilde{x}_n$ denotes the (ANN, DJF, or JJA) average of variable x in year n within the last 10 years of the integration. Regions in the atmosphere where the climate change Δ is statistically significant at the 90% confidence level are shaded in all figures and represent regions where the climate changes are robustly detected and not obscured by natural variability.

3. Climate change in large-scale dynamics

During boreal winter the air in the Arctic that last contacts the midlatitude surface originates primarily over the oceans, owing to vigorous isentropic transport associated with the midlatitude storm tracks; by comparison, during summer, when the storm tracks weaken and large-scale convection over land intensifies, $\Omega_{\rm MID}$ air originates primarily over land (Part I). We therefore analyze the large-scale dynamical response to changes in greenhouse gases in terms of changes in the DJF and JJA climatological zonal winds, meridional transient eddies, and convective cloud fraction (Figs. 1 and 2). As with the air-mass fractions, differences in the dynamical variables are taken between 10-yr REF and FTR climatologies and statistical significance is assessed at the 90% confidence level.

The zonal-mean changes in the wintertime zonal winds, $\Delta[\overline{u}]^{\rm DJF}$ (Fig. 1a), show a poleward and upward shift in the midlatitude jet in response to increases in greenhouse gases, where brackets denote zonal averages. Consistent with phases 3 and 5 of CMIP (CMIP3 and CMIP5) multimodel mean projections the largest zonal wind anomalies are located in the upper troposphere and lower stratosphere, while smaller anomalies near the surface reflect a weaker poleward shift at the surface (e.g., Yin 2005; Woollings and Blackburn 2012; Barnes and Polvani 2013). Owing to the large internal variability of the NH circulation, however, the zonally averaged surface response is not statistically significant.

By comparison, the response aloft is statistically significant and collocated with an intensification in the transient eddy variance of the meridional velocity $\Delta[\overline{v'v'}]^{\rm DJF}$ in the upper troposphere (Fig. 1b), especially on the poleward flank of the tropospheric jet, where eddy activity increases by about 10%. (Primes denote deviations from the time mean and have been calculated using daily mean data, as in Part I.) Similar responses to increases in greenhouse gases have been found in other transient eddy statistics (e.g., transient eddy momentum and heat fluxes), as described in Wu et al. (2011). Note that while $\Delta[\overline{v'v'}]^{\rm DJF}$ has not been bandpass filtered to retain variability on synoptic time scales of 2–8 days as in Wu et al. (2011), we have checked that doing so does not result in a qualitatively different response compared to the unfiltered eddy variance (not shown).

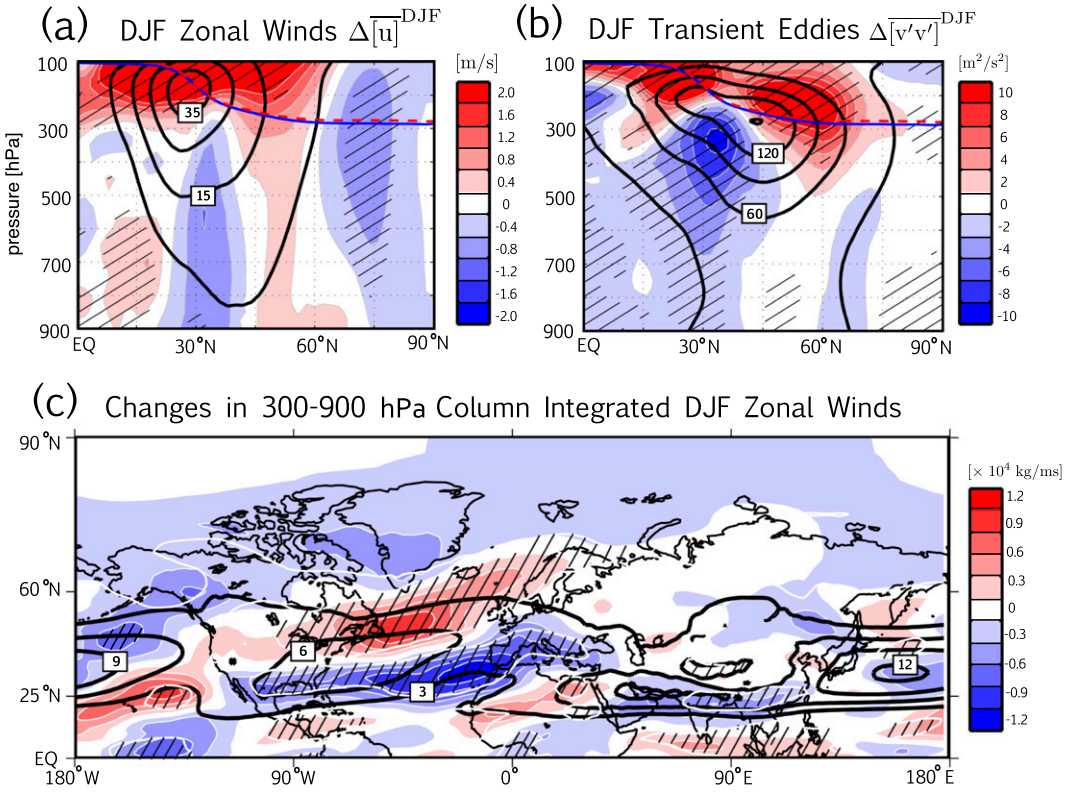

FIG. 1. (a) FTR − REF changes (color shading) in the DJF zonal-mean zonal winds $\Delta\overline{[u]}^{DJF}$. Black contours denote the DJF climatology for the reference climate (contour interval: 10 m s^{-1}). (b) FTR − REF changes (color shading) in the zonally averaged wintertime variance of the meridional eddy velocity $\Delta\overline{[v'v']}^{DJF}$. Climatological values for the REF climate are shown in the black contours (contour interval: 30 m^2 s^{-2}). In both (a) and (b) the REF and FTR wintertime zonal-mean thermal tropopause is shown in the solid blue and dashed red lines, respectively. (c) FTR − REF changes (color shading) in the 300–900-hPa cosine-weighted and column-integrated DJF zonal winds. Thick black contours denote the DJF climatology for the REF climate (contour interval: 3 × 10^4 kg m^{-1} s^{-1}). Regions where the diagnosed climate changes are statistically significant at the 90% confidence level are shown with the gray hatching.

While the zonal-mean response in GEOSCCM indicates that the midlatitude winter circulation will undergo a poleward shift with global warming, an examination of the changes in the DJF 300–900-hPa column-integrated zonal winds reveal strong zonal asymmetries, including a poleward shift over the Atlantic but an equatorward shift over the Pacific (Fig. 1c). Both responses are statistically significant relative to the model's internal variability, although the significance of response over the eastern Pacific is weaker and confined to narrow regions at around 40°N and around 25°N where the zonal winds weaken and intensify, respectively. This response in the model is consistent with projected changes in the NH midlatitude jet among the CMIP5 models (Barnes and Polvani 2013; Delcambre et al. 2013; Simpson et al. 2014).

The response in the NH summer zonal-mean zonal winds, $\Delta\overline{[u]}^{JJA}$ (Fig. 2a), reveals a weakening of the jet throughout the midlatitude troposphere that is mainly significant in the upper troposphere. Changes in the JJA 300–900-hPa column-integrated zonal winds (Fig. 2c), however, show that the zonally averaged changes $\Delta\overline{[u]}^{JJA}$ reflect the near-cancellation of poleward intensified zonal winds over North America and western Europe and a weakening of the jet over the Pacific, consistent with comprehensive climate model projections (Simpson et al. 2014). Of these responses, however, only the weakening of the Pacific jet over the eastern coast of Asia and its intensification over North America are significant relative to the model's internal variability.

Changes in the summertime convective cloud fraction provide a gross sense for how large-scale stability and convective transport over midlatitudes changes in the future climate (preferable to discerning changes in noisier fields, like the vertical velocity ω). The zonal-mean response to changes in greenhouse gases (Fig. 2b) shows a statistically significant decrease in convective cloud fraction throughout the troposphere

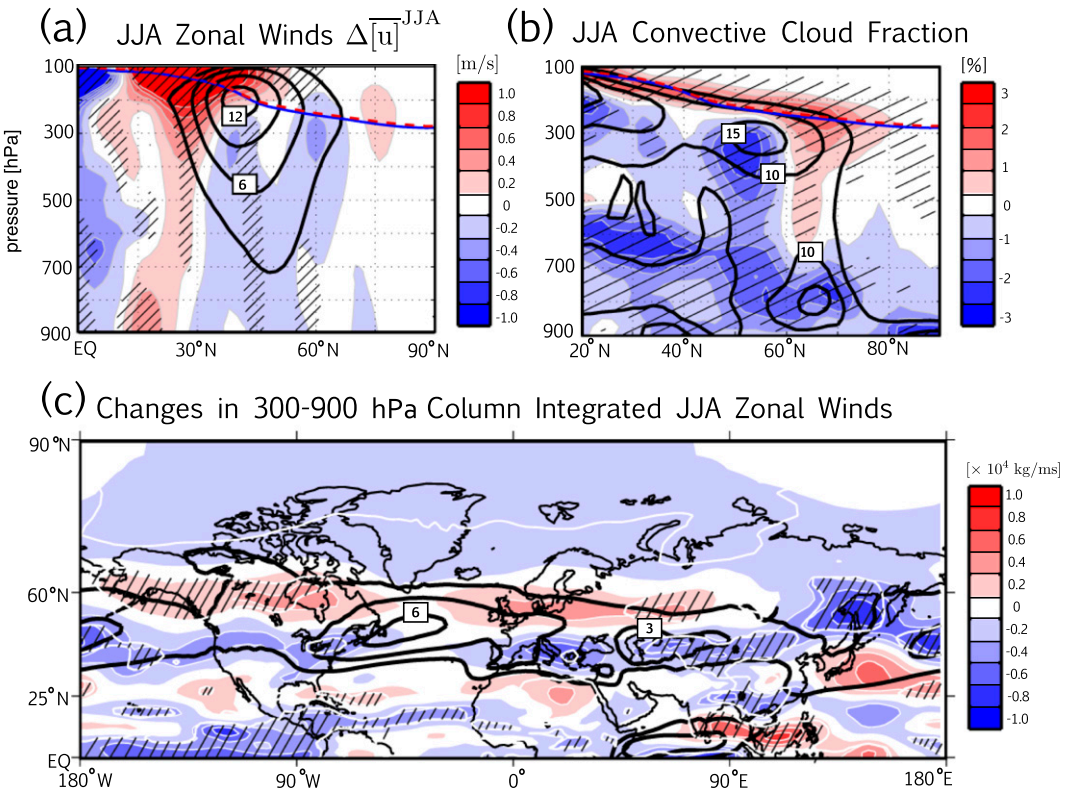

FIG. 2. (a) FTR − REF changes (color shading) in the JJA zonal-mean zonal winds $\Delta\overline{[u]}^{JJA}$. Black contours denote the REF JJA climatology (contour interval: 3 m s^{-1}). (b) The FTR − REF changes (color shading) in the JJA zonally averaged convective cloud fraction, expressed as a percentage (%). Thick black contours denote the JJA REF climatology (contour interval: 5%). (c) FTR − REF changes (color shading) in the 300–900-hPa cosine-weighted and column-integrated JJA zonal winds. Thick black contours denote the REF JJA climatology (contour interval: 3 × 10^4 kg m^{-1} s^{-1}). Regions where the diagnosed climate changes are statistically significant at the 90% confidence level are shown with the gray hatching.

as large-scale vertical motions over the lower and middle troposphere weaken in concert with an increase in tropospheric static stability (Wetherald and Manabe 1988; Senior and Mitchell 1993; Zelinka et al. 2013). In addition, the positive cloud fraction anomalies that extend down from the tropopause poleward of 60°N reflect a poleward shift in the REF climatology, while positive anomalies at the tropopause reflect a deepening of the troposphere as the high-latitude tropopause rises by approximately 10 hPa, consistent with CMIP5 multimodel projections (Zelinka et al. 2013). Finally, smaller-scale convective cloud fraction changes are not discussed as they are not statistically significant and more likely to hinge on model-specific cloud parameterizations and cloud–radiative feedbacks.

4. Climate change in transport to the Arctic

The air-mass fractions have characteristic seasonal-mean climatological distributions and responses to changes in greenhouse gases that we examine systematically in terms of $\Delta\overline{f}^{DJF}$ and $\Delta\overline{f}^{JJA}$. When interpreting the air-mass fraction changes $\Delta\overline{f}$, recall that the air-mass fractions corresponding to last PBL contact over Ω_{STH}, Ω_{MID}, and Ω_{ARC} sum to unity at every point [Eq. (3) in Part I]. Therefore, the sum of their climate changes $\Delta\overline{f}$ is, by construction, zero: $\sum_i \Delta\overline{f}(\mathbf{r}\,|\,\Omega_i) = 0$. Climate change for the air-mass fractions therefore means a change in the relative proportions of the air masses, with an increase in any single air mass always being compensated by decreases in one or more of the other air masses.

During boreal winter and summer, Arctic mid- and upper-tropospheric air originates primarily over the NH midlatitude surface, with $\overline{f}(\mathbf{r}\,|\,\Omega_{MID})$ accounting for 62% (DJF) and 57% (JJA) of the 300–700-hPa column-integrated atmospheric mass poleward of 60°N (Part I). The seasonal-mean responses to increases in greenhouse gases, $\Delta\overline{f}^{DJF}(\mathbf{r}\,|\,\Omega_{MID})$ and $\Delta\overline{f}^{JJA}(\mathbf{r}\,|\,\Omega_{MID})$, reveal that approximately 10% more air will last contact the midlatitude PBL in the future climate both

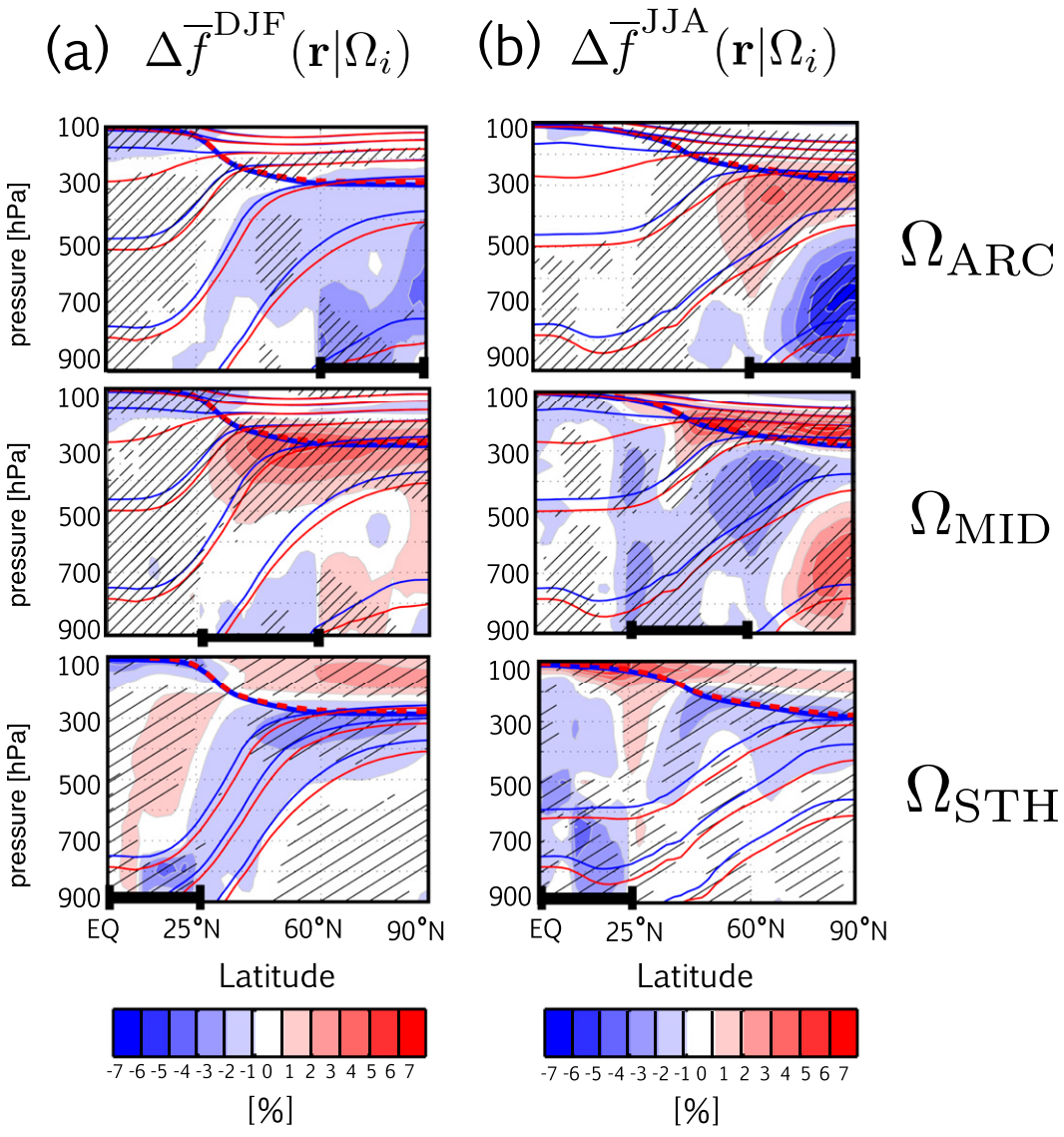

FIG. 3. FTR − REF changes in the fraction of air that last contacted the PBL (top) poleward of 60°N (Ω_{ARC}), (middle) between 25° and 60°N (Ω_{MID}), and (bottom) over latitudes south of 25°N (Ω_{STH}). Changes in the (a) DJF climatological mean air-mass fractions $\Delta\overline{f}^{\mathrm{DJF}}(\mathbf{r}\,|\,\Omega_i)$ and (b) JJA climatological mean air-mass fractions $\Delta\overline{f}^{\mathrm{JJA}}(\mathbf{r}\,|\,\Omega_i)$ are shown. The zonally averaged seasonal mean thermal tropopause is indicated by the solid blue and dashed red lines for the REF and FTR climates, respectively. Seasonal-mean isentropes are overlaid in the thin blue and red lines for the REF and FTR climates, respectively (DJF: 270–390 K, with contour interval of 20 K and JJA: 290–390 K, with contour interval of 20 K). Black bars on the horizontal axis mark the bounds of the PBL origin patches. Regions where the diagnosed climate changes are statistically significant at the 90% confidence level are shown with the gray hatching.

during boreal winter and boreal summer (Fig. 3, middle panels).

The changes $\Delta\overline{f}(\mathbf{r}\,|\,\Omega_{\mathrm{MID}})$ are comparable in magnitude to the 10% increases in tropospheric interhemispheric exchange and mixing times diagnosed in Holzer and Boer (2001) using a climate model, although the focus of that study was not on transport to high latitudes and provides only a qualitative check on the magnitude of the transport responses examined here. Most of the responses are significant at the 90% confidence level, except during boreal winter over latitudes poleward of 80°N within the middle and lower troposphere, where large natural variability precludes a robust climate change signal. While the changes $\Delta\overline{f}^{\mathrm{DJF}}(\mathbf{r}\,|\,\Omega_{\mathrm{MID}})$ and $\Delta\overline{f}^{\mathrm{JJA}}(\mathbf{r}\,|\,\Omega_{\mathrm{MID}})$ both reflect future increases in midlatitude air in the Arctic, large differences in the spatial patterns of the responses,

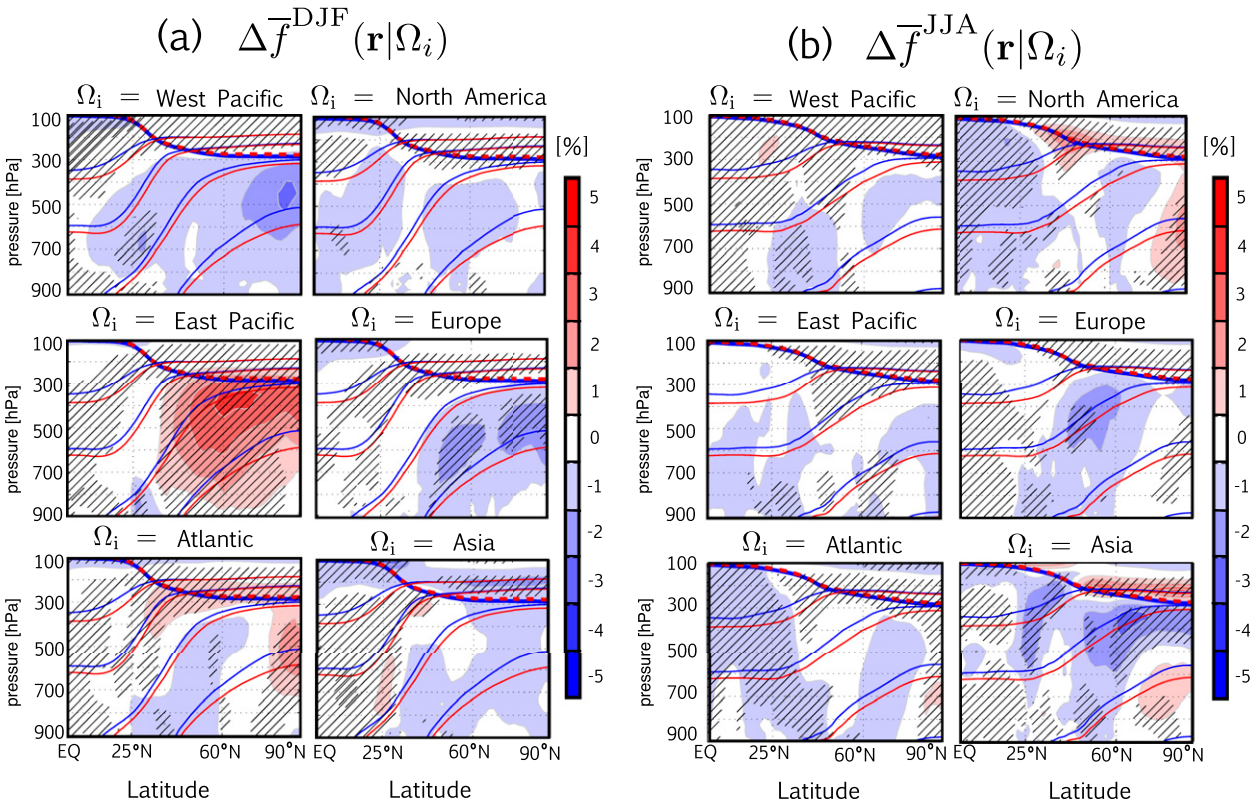

FIG. 4. FTR − REF changes in the fraction of air that last contacted the PBL between 25° and 60°N (Ω_{MID}), further partitioned according to last contact (left) over ocean (i.e., the western Pacific, the eastern Pacific, the Atlantic) and (right) over land (i.e., North America, Europe, and Asia). Future changes (a) in the DJF climatological mean air-mass fractions $\Delta\overline{f}^{\mathrm{DJF}}(\mathbf{r}\,|\,\Omega_i)$ and (b) in the JJA climatological mean air-mass fractions $\Delta\overline{f}^{\mathrm{JJA}}(\mathbf{r}\,|\,\Omega_i)$ are shown. The zonally averaged seasonal mean thermal tropopause for the REF and FTR climates is indicated by the solid blue and dashed red lines, respectively. Seasonal-mean isentropes are overlaid with the thin blue and red lines for the REF and FTR climates, respectively (280–340 K, with contour interval of 20 K). Regions where the diagnosed climate changes are statistically significant at the 90% confidence level are shown with the gray hatching.

however, indicate that different circulation changes are at play. We therefore discuss each season separately.

a. NH winter (DJF)

The large (~7%) positive anomalies in $\Delta\overline{f}^{\mathrm{DJF}}(\mathbf{r}\,|\,\Omega_{\mathrm{MID}})$ that span the midlatitude upper troposphere are mainly compensated by reduced air of southern origin (i.e., Ω_{STH} air) and weaken as they slope isentropically back to the subtropical middle troposphere (Fig. 3a, middle and bottom panels). A comparison of the anomalies in $\Delta\overline{f}^{\mathrm{DJF}}(\mathbf{r}\,|\,\Omega_{\mathrm{MID}})$ with the climatological distribution of $\overline{f}^{\mathrm{DJF}}(\mathbf{r}\,|\,\Omega_{\mathrm{MID}})$ for the reference climate (Fig. A1a, middle panel) indicates that these upper-tropospheric changes reflect the extension of $\overline{f}^{\mathrm{DJF}}(\mathbf{r}\,|\,\Omega_{\mathrm{MID}})$ farther poleward along isentropes in the warmer climate.

The change $\Delta\overline{f}^{\mathrm{DJF}}(\mathbf{r}\,|\,\Omega_{\mathrm{MID}})$ largely reflects increases in air of ocean origin as $\overline{f}^{\mathrm{DJF}}(\mathbf{r}\,|\,\Omega_{\mathrm{EPAC}})$ and $\overline{f}^{\mathrm{DJF}}(\mathbf{r}\,|\,\Omega_{\mathrm{ATL}})$ increase by about 5% and about 3%, respectively (Fig. 4a). The responses $\Delta\overline{f}^{\mathrm{DJF}}(\mathbf{r}\,|\,\Omega_{\mathrm{EPAC}})$ and $\Delta\overline{f}^{\mathrm{DJF}}(\mathbf{r}\,|\,\Omega_{\mathrm{ATL}})$ are statistically significant and are only weakly compensated by reduced fractions of Ω_{WPAC}, Ω_{EUR}, Ω_{NAM}, and Ω_{ASI} air, ensuring that the net change $\Delta\overline{f}^{\mathrm{DJF}}(\mathbf{r}\,|\,\Omega_{\mathrm{MID}})$ is positive. [Note that $\Delta\overline{f}^{\mathrm{DJF}}(\mathbf{r}\,|\,\Omega_{\mathrm{i}})$, summed over all six Ω_i spanning midlatitudes, is equal to the response $\Delta\overline{f}^{\mathrm{DJF}}(\mathbf{r}\,|\,\Omega_{\mathrm{MID}})$ (Fig. 3a, middle panel).] Assuming that air that originates in the marine boundary layer is relatively "clean" compared to air that last contacted the PBL over land, where industrial emissions and biomass burning are large, then our results suggest that future changes in transport alone may reduce Arctic pollution during boreal winter.

The changes $\Delta\overline{f}^{\mathrm{DJF}}(\mathbf{r}\,|\,\Omega_{\mathrm{EPAC}})$ and $\Delta\overline{f}^{\mathrm{DJF}}(\mathbf{r}\,|\,\Omega_{\mathrm{ATL}})$ that span the upper Arctic both reflect upward shifts of the present-day climatological air-mass fractions $\overline{f}^{\mathrm{DJF}}(\mathbf{r}\,|\,\Omega_{\mathrm{EPAC}})$ and $\overline{f}^{\mathrm{DJF}}(\mathbf{r}\,|\,\Omega_{\mathrm{ATL}})$ respectively (Fig. 7a in Part I). As discussed further in section 5 these upper-tropospheric enhancements of oceanic air are located in regions where the zonal-mean upper-tropospheric transient meridional eddies $\overline{[v'v']}^{\mathrm{DJF}}$ intensify (Fig. 1b) and, therefore, most likely reflect enhanced eddy-driven

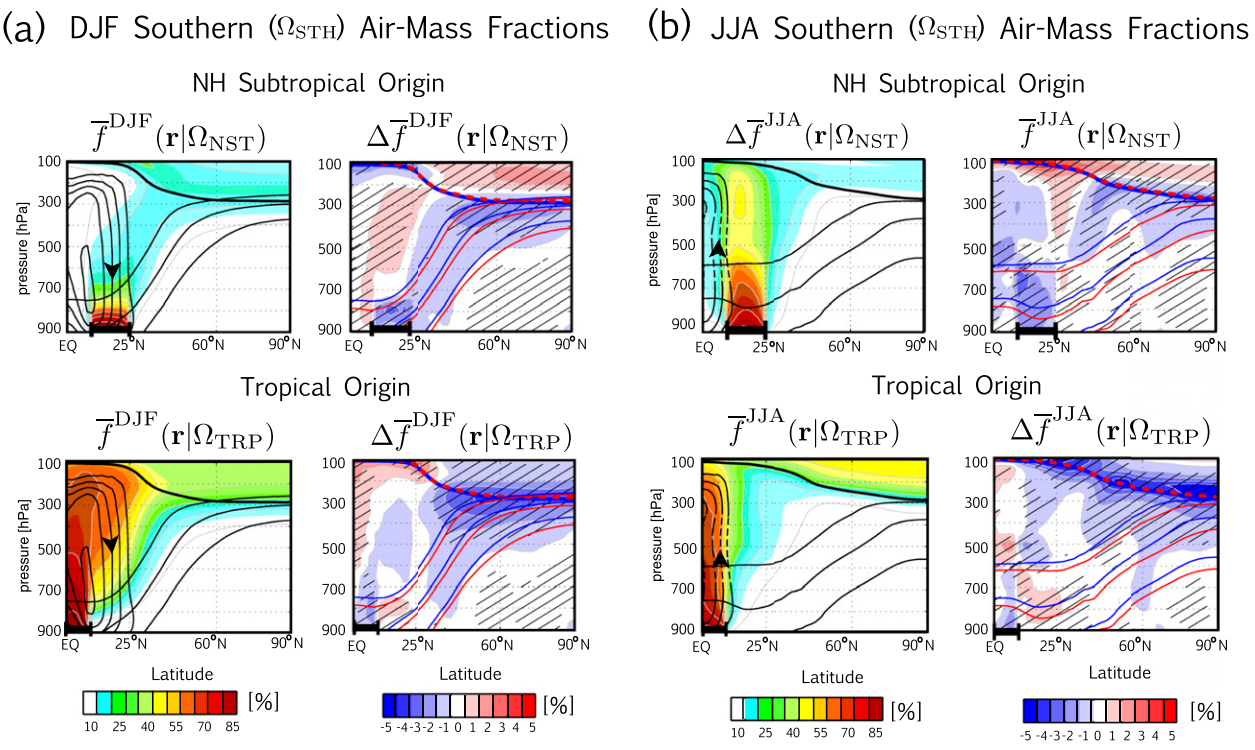

FIG. 5. For both (a) DJF and (b) JJA, the set of four panels shows (top left) the climatological mean air-mass fraction that last contacted the PBL over the Northern Hemisphere subtropics (i.e., Ω_{NST}; 10°–25°N) for the REF climate and (top right) its response to changes in greenhouse gases. In (a), the thin black and blue lines denote the 290-, 300-, and 310-K isentropes for the REF climate; red lines denote the same isentropes, but for the FTR climate. The mean mass streamfunction (contour interval: 60×10^9 kg s^{-1}) has been overlaid in the left panels, in order to provide a sense for the zonally averaged tropospheric circulation in the tropics and subtropics. (bottom) As at (top), but for the air-mass fraction corresponding to last PBL contact over the tropics (i.e., Ω_{TRP}; 10°–10°N). In (b), the 300-, 310-, and 320-K isentropes are shown. Regions where the diagnosed climate changes are statistically significant at the 90% confidence level are shown with the gray hatching.

downgradient transport of Ω_i air higher and farther poleward along isentropes in the warmer climate.

Compared to the upper-tropospheric increases in $\Delta\overline{f}^{DJF}(\mathbf{r}\,|\,\Omega_{EPAC})$ and $\Delta\overline{f}^{DJF}(\mathbf{r}\,|\,\Omega_{ATL})$ that span the Arctic upper troposphere, the anomalies in the lower and middle Arctic troposphere are relatively weaker (~2%–3%) and not statistically significant poleward of 80°N. Equatorward of 80°N the zonal-mean anomalies in $\Delta\overline{f}^{DJF}(\mathbf{r}\,|\,\Omega_{MID})$ are largely compensated by reduced fractions of Ω_{ARC} air (Fig. 3a, top and middle panels) that reflect the flattening of tracer contours on the equatorward edge of Ω_{ARC} (see the climatological distribution of the reference climate $\overline{f}^{DJF}(\mathbf{r}\,|\,\Omega_{ARC})$ in Fig. A1a, top panel). An examination of $\Delta\overline{f}^{DJF}(\mathbf{r}\,|\,\Omega_{ARC})$ in isentropic coordinates (not shown) reveals that these changes reflect not only changes in the isentropes that overlie the polar cap and that warm by approximately 5 K in response to increased GHGs, but also changes in the meridional transport of Ω_{MID} air into the Arctic by large-scale stationary waves over midlatitudes. Changes in large-scale stationary waves over NH midlatitudes are discussed further in section 5a.

In a similar sense we have confirmed that the upper-level changes in $\Delta\overline{f}^{DJF}(\mathbf{r}\,|\,\Omega_{MID})$ do not merely reflect future changes in the isentropes that slope down from the upper Arctic to the subtropical boundary layer and that shift poleward out of Ω_{STH} and into Ω_{MID} in the warmer climate, as such a shift would lead to large compensating anomalies in the air-mass fraction originating at the NH subtropical PBL. Instead, after further decomposing (using additional air-mass fraction tracers) $\Delta\overline{f}^{DJF}(\mathbf{r}\,|\,\Omega_{STH})$ into changes in air of tropical origin (Ω_{TRP}; 10°S–10°N) and air of NH subtropical origin (Ω_{NST}; 10°–25°N), we find that the large positive anomalies of midlatitude air in the upper troposphere are compensated primarily by the negative anomalies in $\Delta\overline{f}^{DJF}(\mathbf{r}\,|\,\Omega_{TRP})$ (Fig. 5a). Since the climatological distribution of $\overline{f}^{DJF}(\mathbf{r}\,|\,\Omega_{TRP})$ in the Arctic primarily reflects transport processes in the tropical upper troposphere and extratropical lower stratosphere (Fig. 5a, bottom-left panel), the changes in midlatitude air in the upper

Arctic, therefore, are most likely the responses to circulation changes in the upper troposphere, not merely shifts in isentropes.

b. NH summer (JJA)

In contrast to winter, the summertime response to increases in greenhouse gases, $\Delta\overline{f}^{\mathrm{JJA}}(\mathbf{r}\,|\,\Omega_{\mathrm{MID}})$, features a dipole of statistically significant positive anomalies in the lower Arctic flanked by negative anomalies aloft (Fig. 3b, middle panel). In the middle and upper Arctic, the reduced fractions of Ω_{MID} air are mainly compensated by positive anomalies in $\Delta\overline{f}^{\mathrm{JJA}}(\mathbf{r}\,|\,\Omega_{\mathrm{ARC}})$ that extend down to the lower troposphere along the equatorward edge of Ω_{ARC}. These increases in Ω_{ARC} air, when compared to the climatological distribution of $\overline{f}^{\mathrm{JJA}}(\mathbf{r}\,|\,\Omega_{\mathrm{ARC}})$ for the reference climate (Fig. A1b, top panel), reflect the tendency for air labeled on the equatorward edge of Ω_{ARC} to penetrate farther across isentropes into the upper troposphere in the warmer climate.

To interpret the changes $\Delta\overline{f}^{\mathrm{JJA}}(\mathbf{r}\,|\,\Omega_{\mathrm{MID}})$ we further partition $\overline{f}^{\mathrm{JJA}}(\mathbf{r}\,|\,\Omega_{\mathrm{MID}})$ into air that last contacted the PBL over ocean and over land. Recall from Part I that during boreal summer midlatitude air originates primarily over land, with $\overline{f}^{\mathrm{JJA}}(\mathbf{r}\,|\,\Omega_{\mathrm{ASI}})$ and $\overline{f}^{\mathrm{JJA}}(\mathbf{r}\,|\,\Omega_{\mathrm{NAM}})$ respectively accounting for 41% and 24% of the 300–700-hPa column-integrated Ω_{MID} air-mass fraction poleward of 60°N. Thus, not surprisingly, the anomalies in $\Delta\overline{f}^{\mathrm{JJA}}(\mathbf{r}\,|\,\Omega_{\mathrm{MID}})$ primarily reflect changes in the air-mass fractions originating over North America and over Asia (Fig. 4b). In particular, the positive anomalies in $\Delta\overline{f}^{\mathrm{JJA}}(\mathbf{r}\,|\,\Omega_{\mathrm{MID}})$ that span the lower and middle Arctic poleward of 70°N mainly reflect an increase in $\overline{f}^{\mathrm{JJA}}(\mathbf{r}\,|\,\Omega_{\mathrm{NAM}})$ that is statistically significant; by comparison, the positive anomalies in $\overline{f}^{\mathrm{JJA}}(\mathbf{r}\,|\,\Omega_{\mathrm{ASI}})$ are weak and not significant over the polar cap. As discussed further in section 5b, the fact that the lower Arctic changes in $\Delta\overline{f}^{\mathrm{JJA}}(\mathbf{r}\,|\,\Omega_{\mathrm{ASI}})$ appear weaker, however, is due mainly to zonally averaging large compensating negative and positive anomalies over different longitudinal bands in the Arctic. In fact, localized increases in Ω_{ASI} air at places exceed 15%.

By comparison, the negative anomalies in $\Delta\overline{f}^{\mathrm{JJA}}(\mathbf{r}\,|\,\Omega_{\mathrm{MID}})$ equatorward of 70°N that extend into the upper Arctic primarily reflect a decrease in the air-mass fraction originating over Asia. These decreases in Asian air are statistically significant poleward of 60°N and are interpreted partly as the response to the poleward shift in convection. That is, as convection shifts poleward in the warmer climate, there is stronger (weaker) convective transport of Ω_{ARC} (Ω_{ASI}) air into the upper troposphere over middle and high latitudes. Similar responses to a weakening in large-scale convection over midlatitudes can be seen in the response of the Ω_{EUR} air-mass fraction (Fig. 4b). However, these anomalies barely penetrate north of 60°N and are not discussed further.

Finally, the thin band of large (~7%) and statistically significant anomalies in $\Delta\overline{f}^{\mathrm{JJA}}(\mathbf{r}\,|\,\Omega_{\mathrm{MID}})$ at the Arctic tropopause (Fig. 3b, middle panel) is compensated primarily by negative anomalies in the Ω_{STH} air-mass fraction (Fig. 3b, bottom panel). Further partitioning $\Delta\overline{f}^{\mathrm{JJA}}(\mathbf{r}\,|\,\Omega_{\mathrm{STH}})$ into PBL origin over the tropics and over the NH subtropics reveals that the increases in Ω_{MID} air are compensated primarily by negative anomalies in air of tropical origin, $\Delta\overline{f}^{\mathrm{JJA}}(\mathbf{r}\,|\,\Omega_{\mathrm{TRP}})$ (Fig. 5b, right panels). Given that $\overline{f}^{\mathrm{JJA}}(\mathbf{r}\,|\,\Omega_{\mathrm{TRP}})$ features strong vertical gradients in the Arctic upper troposphere/lower stratosphere and that the anomalies in $\Delta\overline{f}^{\mathrm{JJA}}(\mathbf{r}\,|\,\Omega_{\mathrm{TRP}})$ are more or less confined to the tropopause, the changes $\Delta\overline{f}^{\mathrm{JJA}}(\mathbf{r}\,|\,\Omega_{\mathrm{MID}})$ most likely reflect the 10-hPa rise in tropopause height in the warmer climate.

5. Changes in PBL origin of Arctic air: Large-scale circulation constraints

To aid in the interpretation of the air-mass-fraction responses to future warming, we now discuss changes in the large-scale circulation over the midlatitudes, including changes in large-scale stationary waves, transient eddy variance, and large-scale convection. Throughout, we focus on circulation changes that GEOSCCM represents with fidelity compared to other comprehensive climate models subject to A1B GHG forcing (i.e., the dynamical changes discussed in section 2).

a. Enhanced oceanic PBL origin during NH winter

Recall from Part I that the Ω_{MID} air-mass fraction in the lower Arctic reflects transport by large-scale stationary waves over NH midlatitudes that control the low-level convergence and poleward transport of recently labeled Ω_{MID} air into the Arctic. More precisely, it is shown that the individual Ω_{MID} air-mass fractions originating over regions of mean cyclonic flow tend to be large over their corresponding origin regions Ω_i, since low-level convergence ensures that air is less likely to relabeled elsewhere at the PBL. In addition to modifying the conditions under which air is (re)labeled at the PBL, changes in large-scale stationary waves also affect meridional transport into the Arctic. Thus, when interpreting the changes $\Delta\overline{f}^{\mathrm{DJF}}(\mathbf{r}\,|\,\Omega_{\mathrm{i}})$ in the lower troposphere it is important to consider both changes in low-level convergence and the meridional flow aloft relative to the underlying surface origin regions.

To begin, we examine the NH winter sea level pressure (SLP) response to increases in greenhouse gases.

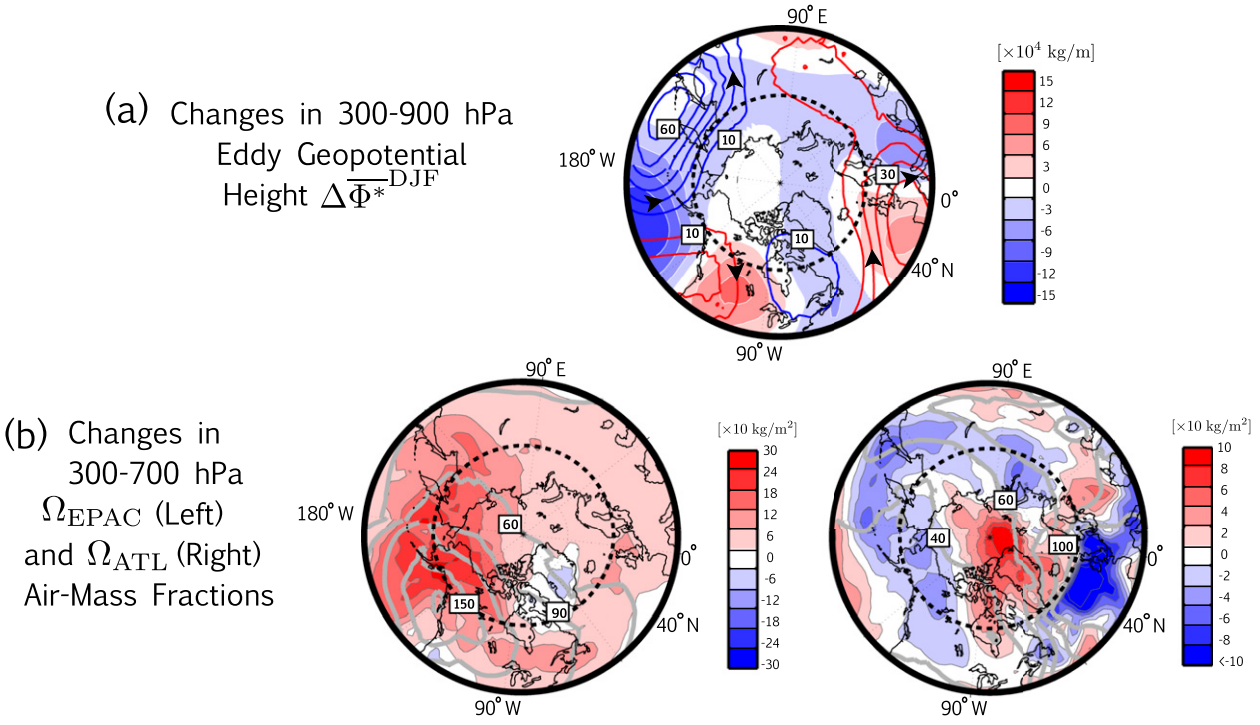

FIG. 6. (a) FTR − REF changes (color shading) in the DJF climatological mean 300–900-hPa column-integrated eddy geopotential height $\Delta\overline{\Phi^*}^{\mathrm{DJF}}$. Color contours show the climatology for the reference climate (contour interval: 10×10^4 kg m^{-1}). (b) FTR − REF changes (color shading) in the 300–700-hPa column-integrated air-mass fractions that last contacted the PBL over the eastern Pacific and the Atlantic, (left) $\Delta\overline{f}^{\mathrm{DJF}}(\mathbf{r}\,|\,\Omega_{\mathrm{EPAC}})$ and (right) $\Delta\overline{f}^{\mathrm{DJF}}(\mathbf{r}\,|\,\Omega_{\mathrm{ATL}})$. The thick gray contours show the climatological mean air-mass fractions for the REF climate; contour interval is 300 kg m^{-2} in (left) and 200 kg m^{-2} in (right). In all panels the thick dashed circle marks the beginning of the Arctic region at 60°N and latitudes up to 40°N are shown.

Over the Pacific the Aleutian low deepens by approximately 3 hPa (Fig. A2a, left panel), a response that closely resembles the sea level pressure changes that occur during El Niño (Trenberth and Hurrell 1994; Zhang et al. 1997). This response is consistent with CMIP3 and CMIP5 multimodel projections, some of which reveal sea level pressure decreases over the North Pacific in excess of 4 hPa (IPCC 2013). As the Aleutian low deepens, low-level convergence and mean ascent shifts farther over Ω_{EPAC}. Associated with these changes, the near-surface westerlies weaken over the eastern Pacific and obtain a more northward component over Alaska, ensuring that Ω_{EPAC} air in the warmer climate is less likely to be advected westward over North America, where it is relabeled (Fig. A2b, left panel). Correspondingly, large positive anomalies in $\Delta\overline{f}^{\mathrm{DJF}}(\mathbf{r}\,|\,\Omega_{\mathrm{EPAC}})$ overlie Ω_{EPAC} and extend poleward over Alaska and Canada (Fig. A2c, left panel). Note that the weaker westerlies over the Pacific are a statistically significant response to increased GHGs in our model (Fig. 1c).

In addition to the wind changes that impact the (re)labeling of eastern Pacific air at the PBL, we find that the near-surface wind response over the Pacific is associated with a barotropic cyclonic anomaly that extends throughout the troposphere. This circulation anomaly is manifest as negative anomalies in the 500–900-hPa-integrated eddy geopotential height $\Delta\overline{\Phi^*}^{\mathrm{DJF}}$ (Fig. 6a), which give the mean wind along the west coast of North America a stronger and more northward component. In turn, consistent with stronger poleward flow aloft, there are significant increases in the 300–700-hPa-integrated Ω_{EPAC} air-mass fraction over the Arctic that at some places (e.g., Alaska) represent nearly a 25% relative increase compared to the REF climate (Fig. 6b, left panel). We note that while this cyclonic circulation anomaly is associated with an equatorward displacement of the eastern Pacific storm track (Fig. 1c), both the jet shift and the increases in $\Delta\overline{f}^{\mathrm{DJF}}(\mathbf{r}\,|\,\Omega_{\mathrm{EPAC}})$ are manifestations of changes in the large-scale stationary wave flow so that the anomalies in $\Delta\overline{f}^{\mathrm{DJF}}(\mathbf{r}\,|\,\Omega_{\mathrm{EPAC}})$ are not necessarily a direct response to a shift in the tropospheric jet.

Over the Atlantic, by comparison, the sea level pressure response reveals a westward and northward shift in the Icelandic low out of midlatitudes and over

Greenland, consistent with CMIP3 and CMIP5 multimodel mean projections, which results in lower pressures over the poles and higher pressures over midlatitudes (i.e., a trend in the northern annular mode toward its high index polarity) (Thompson et al. 2000) (Fig. A2a, right panel). This is associated with stronger westerlies over the North Atlantic, a statistically significant response relative to the model's internal variability (Fig. A2b, right panel, and Fig. 1c). Correspondingly, stronger westerlies ensure that Ω_{ATL} air is less likely to encounter its origin region and more likely to be advected east over Europe, where it is relabeled, resulting in the negative anomalies in $\Delta\overline{f}^{DJF}(\mathbf{r}\,|\,\Omega_{ATL})$ over the Atlantic (Fig. 5b and Fig. A2c, right panel).

As over the Pacific, the stationary wave response over the Atlantic is not confined to the surface but rather is related to a barotropic anticyclonic anomaly that extends throughout the lower and middle troposphere over the eastern Atlantic and western coast of Europe. This circulation feature appears as positive anomalies in the 300–700-hPa column-integrated eddy geopotential height and projects strongly onto the REF climatology (Fig. 6a). Correspondingly, enhanced longitudinal gradients in $\overline{\Phi^*}^{DJF}$ (i.e., stronger geostrophic meridional flow) over the North Atlantic ensure that Ω_{ATL} air is more likely to be transported poleward and less likely to be advected eastward by the mean westerlies, resulting in lower-tropospheric positive anomalies in $\Delta\overline{f}^{DJF}(\mathbf{r}\,|\,\Omega_{ATL})$ that span the polar cap (Fig. 6b, right panel).

Finally, while changes in large-scale stationary waves over the NH appear to control much the response of the Ω_i air-mass fractions in the lower and middle troposphere, in the upper Arctic (i.e., above 500 hPa) interactions with the PBL are weaker and the poleward transport of Ω_i air during winter is largely mediated by the transient eddy variance of the meridional velocity (Part I). More precisely, by recasting the passive tracer equation in terms of the residual mean circulation we show in Part I that the eddy transport term $\overline{\partial v' f'(\Omega_i)/\partial y}^{DJF}$ is much larger than the transport by the mean circulation, that is, $\overline{v^*\partial[f(\Omega_i)]/\partial y}^{DJF}$, where stars denote deviations from the zonal mean. For that reason, it is useful to compare the changes in these individual terms when interpreting upper-level changes in the Ω_{EPAC} and Ω_{ATL} air-mass fractions. (Note that, as in Part I, we are not performing rigorous budget calculations. We are merely interested in comparing changes in the relative importance of the two meridional transport terms).

A comparison of $\Delta\overline{\partial[v'f'(\Omega_i)]/\partial y}^{DJF}$ and $\Delta\overline{v^*\partial[f(\Omega_i)]/\partial y}^{DJF}$ (Fig. 7) for the Ω_{EPAC} air-mass fraction reveals that future changes in eddy-driven transport largely dominate changes in transport by the advective component of the flow. Positive changes in $\Delta\overline{\partial[v'f'(\Omega_i)]/\partial y}^{DJF}$ are more or less confined to the midlatitude and Arctic upper troposphere, where transient eddies of the meridional wind increase in the future climate. We also find a similar response in the budget of the Ω_{ATL} air-mass fraction throughout the troposphere, although this comparison is not shown for sake of brevity. These results suggest that the enhancement of oceanic air in the upper Arctic is most likely a response to more vigorous meridional eddies, which shift upward and poleward in response to increases in greenhouse gases (Fig. 1b).

b. Enhanced land PBL origin during NH summer

Air that is labeled over Ω_{ASI} and convectively lifted out of the PBL during boreal summer is either transported equatorward to the subtropical upper troposphere via the Asian monsoon or eastward across the Pacific by the mean westerly flow (see Fig. 11, left panel, in Part I). As shown in Part I, strong poleward flow over Siberia ensures that Ω_{ASI} air that is convectively transported out of the PBL first enters the Arctic before crossing the Pacific, resulting in the large fractions of Ω_{ASI} air that dominate the Arctic middle and upper troposphere. By comparison, Ω_{NAM} air is deflected southward away from the Arctic by mean equatorward flow and is more likely to be relabeled at the PBL, resulting in weaker fractions $\overline{f}^{JJA}(\mathbf{r}\,|\,\Omega_{NAM})$ compared to $\overline{f}^{JJA}(\mathbf{r}\,|\,\Omega_{ASI})$ (see Fig. 11, right panel, in Part I).

In response to increases in greenhouse gases, convection shifts poleward into the equatorward edge of Ω_{ARC} (Fig. 2b), with most of this shift occurring over Europe and Asia (not shown). Correspondingly, as convection shifts poleward less Ω_{ASI} air is vertically lofted away from the PBL into the upper troposphere, consistent with an overall reduction in $\overline{f}^{JJA}(\mathbf{r}\,|\,\Omega_{ASI})$ throughout most of the NH midlatitude and subtropical troposphere (Fig. 4b). As convection shifts over the Arctic, the negative anomalies in $\Delta\overline{f}^{JJA}(\mathbf{r}\,|\,\Omega_{ASI})$ are compensated by increased fractions of Ω_{ARC} air (Fig. 3b, top panel).

To interpret the positive anomalies in $\overline{f}^{JJA}(\mathbf{r}\,|\,\Omega_{ASI})$ that overlie the Arctic lower and middle troposphere we consider not only changes in transport out of the Asian PBL but also changes in the meridional transport of Ω_{ASI} air into the Arctic. In response to increases in greenhouse gases the large positive and negative anomalies of the 500–900-hPa column-integrated eddy geopotential height $\Delta\overline{\Phi^*}^{JJA}$ (Fig. 8a) over northern Russia imply stronger poleward flow over Siberia. Correspondingly, large positive anomalies in $\Delta\overline{f}^{JJA}(\mathbf{r}\,|\,\Omega_{ASI})$ over Siberia extend over the polar cap, representing at

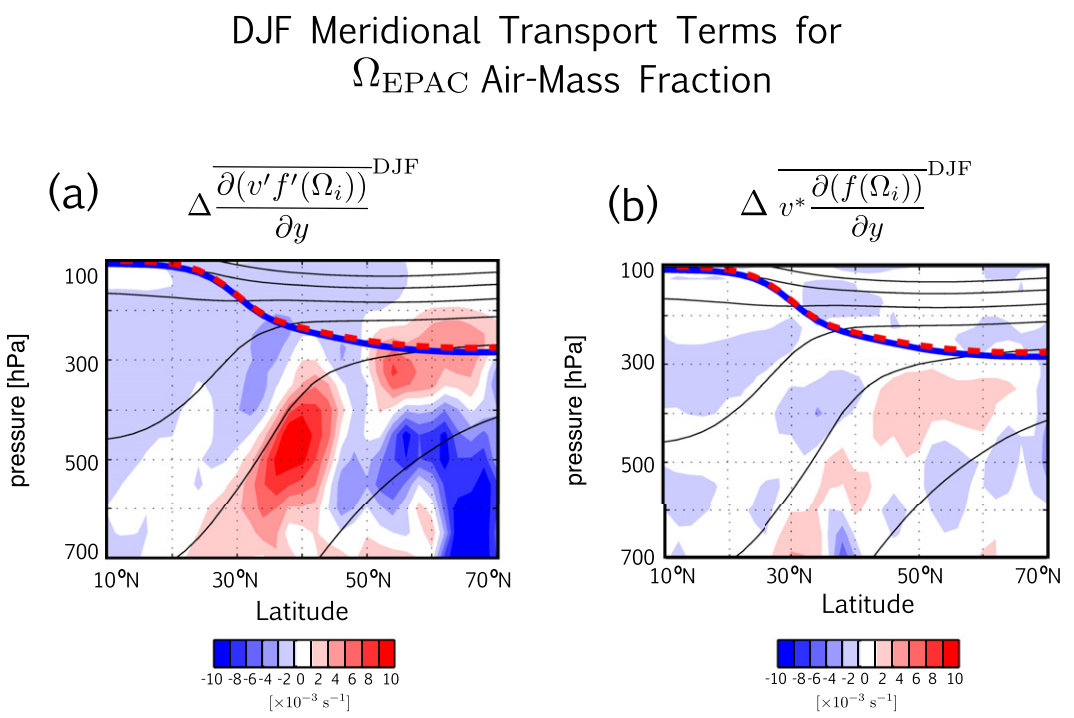

FIG. 7. Comparison of FTR − REF changes in the DJF climatological eddy-induced and residual mean transport terms, (a) $\Delta\overline{\partial[v'f'(\Omega_i)]/\partial y}^{\mathrm{DJF}}$ and (b) $\Delta\overline{v^*\partial[f(\Omega_i)]/\partial y}^{\mathrm{DJF}}$, for air that last contacted the PBL over the eastern Pacific. Thin black lines denote the zonal-mean DJF isentropes for the REF climate (contour interval: 30 K). The REF and FTR zonal-mean boreal winter thermal tropopause is indicated in both panels by the solid blue and dashed red lines, respectively.

places 10%–15% relative increases compared to the REF climate (Fig. 8b, left panel). Strong negative anomalies in $\Delta\overline{f}^{\mathrm{JJA}}(\mathbf{r}\,|\,\Omega_{\mathrm{ASI}})$ over North America, however, render the zonal-mean response only weakly positive (Fig. 5b).

The changes in $\Delta\overline{\Phi^*}^{\mathrm{JJA}}$ (Fig. 8a) may also be used to interpret changes in the 500–900-hPa column-integrated air-mass fraction $\overline{f}^{\mathrm{JJA}}(\mathbf{r}\,|\,\Omega_{\mathrm{NAM}})$ (Fig. 8b, right panel). In particular, large increases in Ω_{NAM} air over Greenland and Canada (at places ~20% relative increases compared to the REF climate) are flanked eastward by large negative anomalies over Scandinavia, similarly leading to only weakly positive zonal-mean changes (Fig. 4b). The increased fractions of Ω_{NAM} air that span the lower Arctic over Greenland indicate that as the Atlantic jet shifts poleward (Fig. 2c) Ω_{NAM} air is less likely to be drawn eastward over the Atlantic (where it is relabeled) and more likely to enter the Arctic via the North Atlantic, where the mean flow is poleward.

6. Conclusions

There is growing evidence that changes in the long-range transport of midlatitude pollutants have impacted Arctic climate over recent decades (e.g., Hansen and Nazarenko 2004; Lubin and Vogelmann 2006; Shindell et al. 2008). It is therefore natural to ask how long-range transport from midlatitudes to the Arctic will respond to large-scale circulation changes over the twenty-first century. Here, we have assessed how the composition of Arctic air (in terms of its last PBL origin) changes in response to increases in greenhouse gases. Changes in the air-mass fractions reveal the following:

1) Our model projections indicate that (~10%) more air in the Arctic will originate at the NH midlatitude PBL. The largest increases of midlatitude air during NH winter are concentrated in the upper and middle Arctic, where they reflect an intensification of the transient eddy meridional wind that shifts poleward and upward in response to future increases in greenhouse gases. During summer, by comparison, enhanced fractions of midlatitude air are concentrated below 500 hPa and extend down to the Arctic surface.
2) Increased fractions of midlatitude air during winter primarily reflect increases in air of eastern Pacific and Atlantic origin, indicating that transport changes alone in the future may lead to "cleaner" Arctic winters (i.e., less air from polluted boundary layers

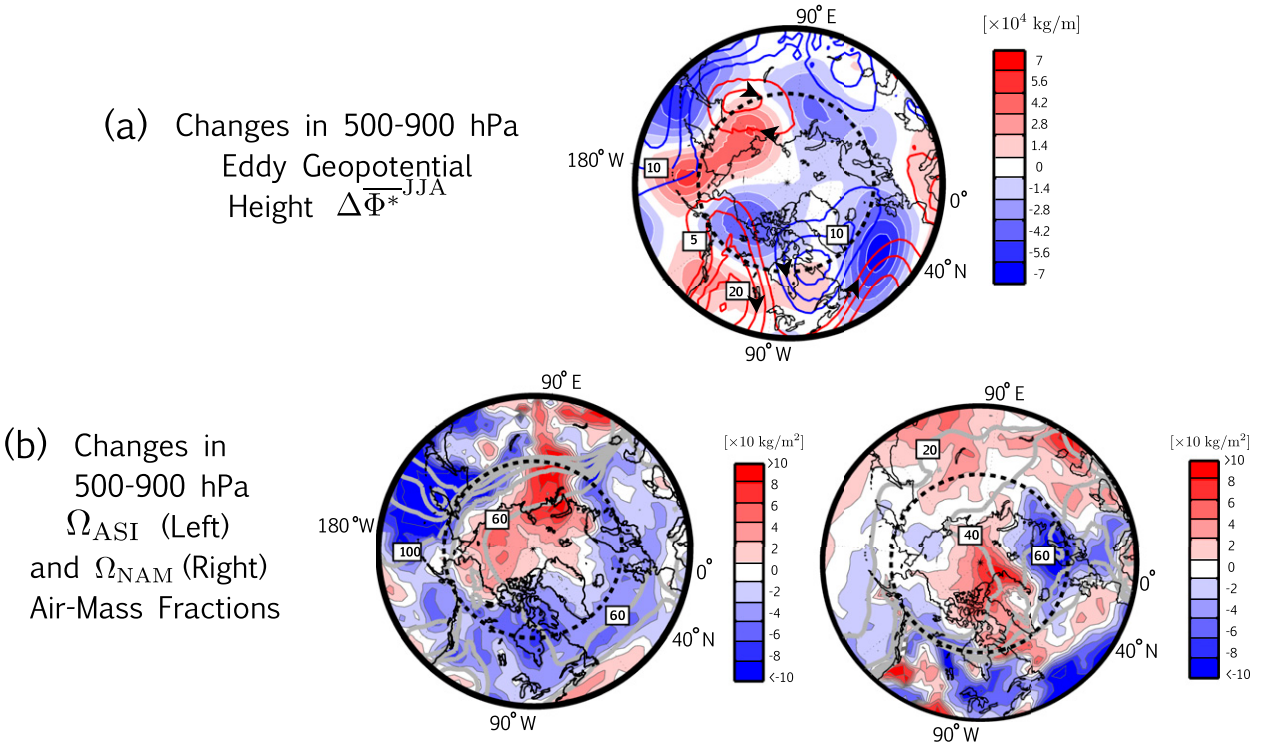

FIG. 8. (a) FTR − REF changes (color shading) in the JJA climatological mean 500–900-hPa column-integrated eddy geopotential height $\Delta\overline{\Phi^*}^{JJA}$. Color contours show the climatology for the reference climate (contour interval: 5×10^4 kg m^{-1}). (b) FTR − REF changes (color shading) in the 500–900-hPa column-integrated air-mass fractions that last contacted the PBL over Asia and North America, (left) $\Delta\overline{f}^{JJA}(\mathbf{r} \mid \Omega_{ASI})$ and (right) $\Delta\overline{f}^{JJA}(\mathbf{r} \mid \Omega_{NAM})$. The thick gray contours show the climatological mean air-mass fractions for the REF climate; contour interval is 200 kg m^{-2} in both panels. In all panels the thick dashed circle marks the beginning of the Arctic region at 60°N and latitudes up to 40°N are shown.

over industrial regions). Future increases in air of eastern Pacific PBL origin reflect anomalous poleward flow along the west coast of North America, a robust dynamical response among comprehensive climate models.

3) The NH summer air-mass origin response to increases in GHGs is characterized by about 5% increases in air of Asian and North American PBL origin throughout the lower and middle Arctic, indicating that transport changes may enhance Arctic pollution during summer. The enhanced fractions of Asian air are consistent with weaker large-scale convection over NH midlatitudes and stronger poleward flow over Siberia so that less Ω_{ASI} air is convectively transported southward into the subtropical upper troposphere and more efficiently steered poleward into the Arctic.

Enhanced poleward transport of midlatitude air may have various impacts on climate by modifying the radiative and chemical properties of the Arctic. Our results indicate that this will depend strongly on season, with higher fractions of oceanic air that are relatively diluted in anthropogenic aerosols dominating the NH winter response; conversely, increases in air originating over Asia, where there are large industrial emissions, could lead to enhanced aerosol loading during summer. To further relate the species-independent transport diagnostics presented here to particulate and gaseous tracers (e.g., black carbon and hydrocarbons) we plan on expanding our analysis using tracers similar to the Ω_i air-mass fractions, but also subject to idealized chemical and/or physical loss.

When relating our results to studies of pollution transport, other considerations must be made, including how processes within the PBL may impact chemical constituents. In this study the air-mass fractions, by construction, track air since last PBL contact and air that travels low-level paths into the Arctic become relabeled as Arctic air along the way. However, while our boundary region Ω has been defined for convenience as the modeled PBL, the choice of Ω may be refined to account for species that are sensitive to transport pathways within the PBL. For example, one may be interested in examining the surface origin of short-lived ozone depleting substances residing in the tropical upper troposphere that may be sensitive to low-level

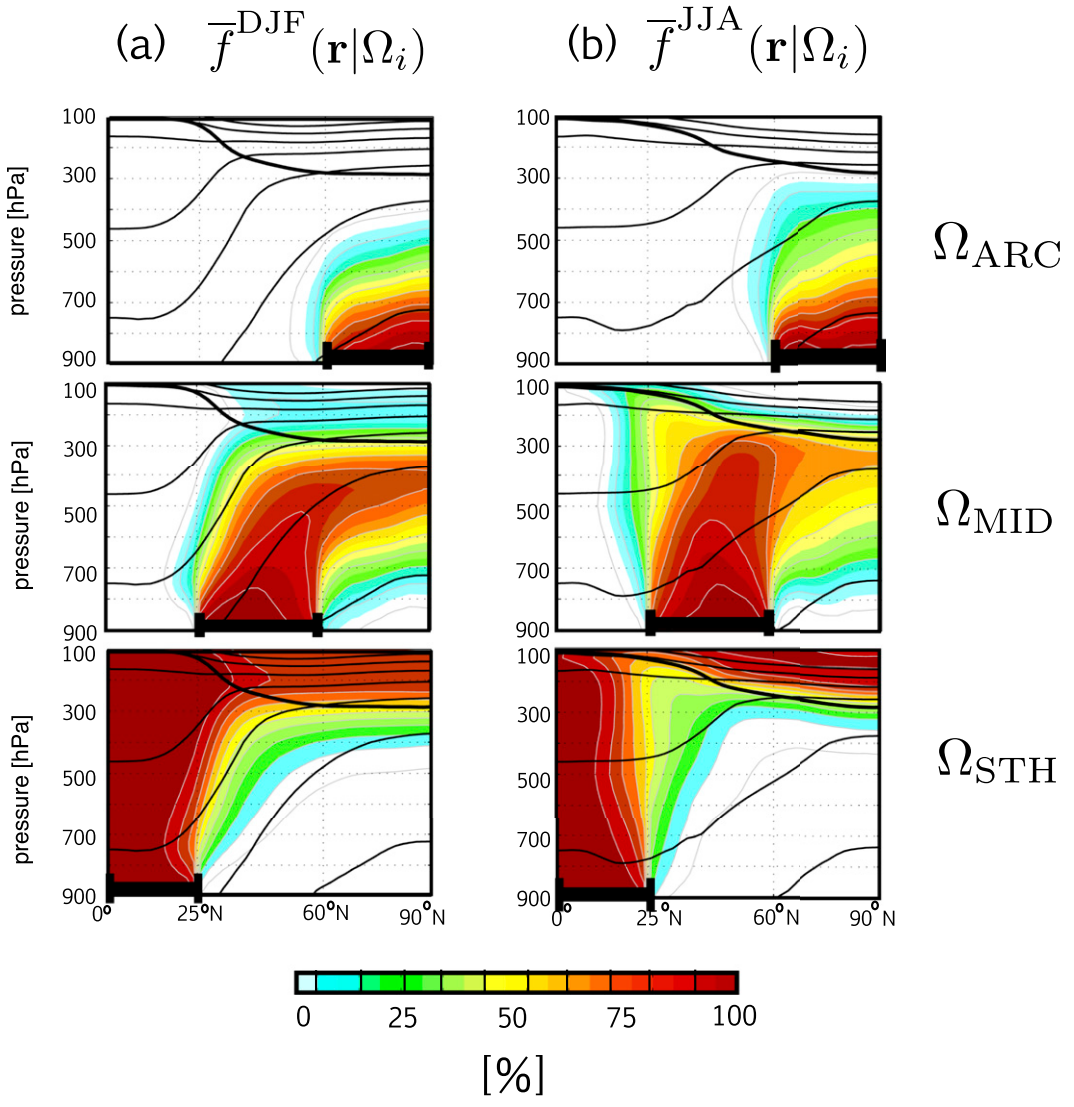

FIG. A1. The fraction of air that last contacted the PBL over (top) Ω_{ARC}, (middle) Ω_{MID}, and (bottom) Ω_{STH}. DJF and JJA climatological mean air-mass fractions (a) $\overline{f}^{\mathrm{DJF}}(\mathbf{r}\,|\,\Omega_i)$ and (b) $\overline{f}^{\mathrm{JJA}}(\mathbf{r}\,|\,\Omega_i)$ are shown, respectively. The zonally averaged seasonal mean thermal tropopause is indicated by the thick black line. Seasonal-mean isentropes are overlaid in black [20-K contour interval for isentropes between 270 and 390 K (DJF) and between 290 and 390 K (JJA)]. Modified from Fig. 5 of Part I.

cross-equatorial paths associated with seasonal changes in tropical convection, in which case it may be appropriate to use zero-flux boundary conditions over part of Earth's surface and/or mixing-ratio boundary conditions that are rapidly pulsed in time (Holzer 2009).

When considering future changes in tropospheric chemical composition, it may also be important to keep track of the relative amounts of air that are of tropospheric and stratospheric origin. This would be relevant to ozone, for example, which has both tropospheric and stratospheric sources. While the air-mass fractions defined here trace all air back to its last contact with the PBL, one can readily generalize the setup to also include stratospheric regions of last contact (e.g., Orbe et al. 2013) so that the air-mass fractions sum to unity only when both tropospheric and stratospheric fractions are included. A future decrease in the mass exchange between the PBL and the free troposphere would manifest as a decrease in the PBL air-mass fraction with a corresponding increase in the stratospheric fraction.

Finally, the modeled transport response in GEOSCCM underscores how longitudinal variations in the NH midlatitude circulation response to climate change may lead to significantly different regional

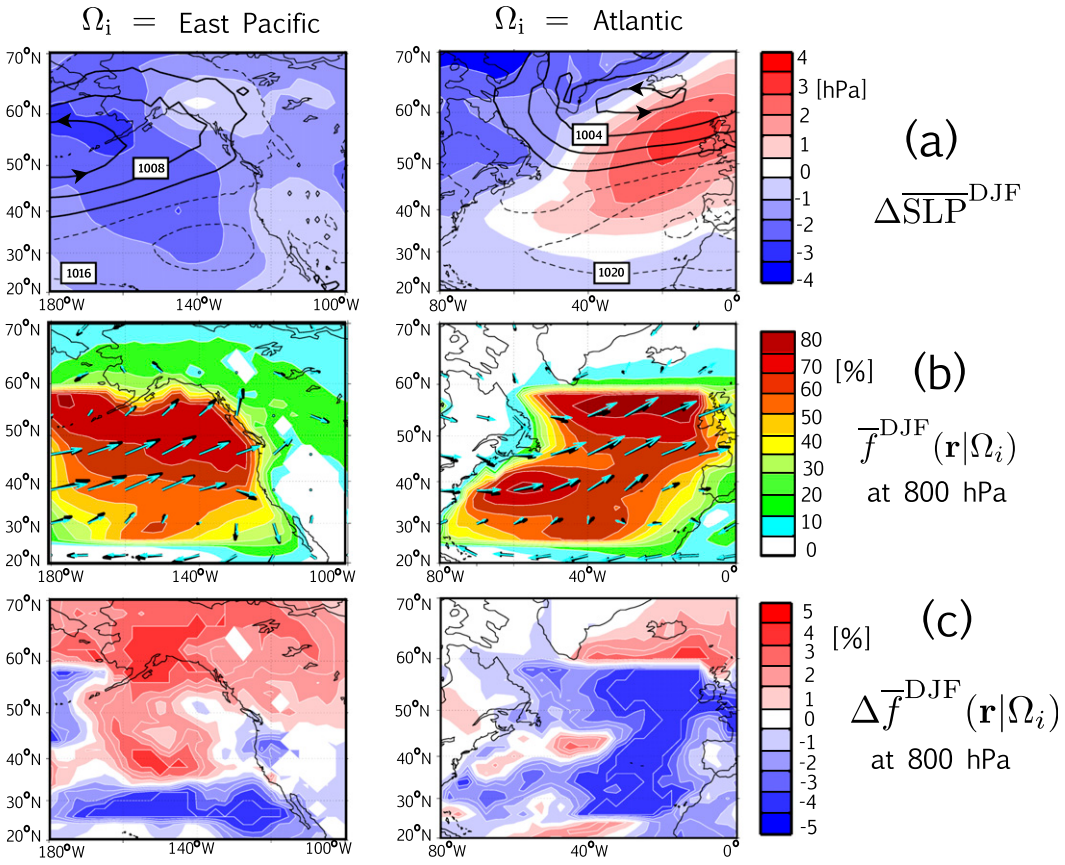

FIG. A2. (a) FTR − REF changes in the DJF climatological mean sea level pressure $\Delta\overline{\mathrm{SLP}}^{\mathrm{DJF}}$ shown over the (left) eastern Pacific and (right) Atlantic. Black contours denote the climatology for the REF integration. (b) The DJF climatological mean air-mass fraction that last contacted the PBL at midlatitudes over the (left) eastern Pacific and (right) Atlantic evaluated at 800 hPa for the REF climate. The cosine-weighted DJF climatological mean 800-hPa winds are shown in the arrows for the REF climate (black) and FTR climate (cyan). (c) The FTR − REF changes in the DJF climatological mean air-mass fractions that last contacted the PBL over the eastern Pacific and Atlantic for (left) $\Delta\overline{f}^{\mathrm{DJF}}(\mathbf{r}\,|\,\Omega_{\mathrm{EPAC}})$ and (right) $\Delta\overline{f}^{\mathrm{DJF}}(\mathbf{r}\,|\,\Omega_{\mathrm{ATL}})$, respectively, also evaluated at 800 hPa.

responses in meridional transport. In particular, our results show that, while the zonal-mean midlatitude jet is projected to shift poleward in response to increases in greenhouse gases, the dominant transport response—enhanced fractions of eastern Pacific air—is linked to projected changes in large-scale stationary waves in the Pacific where the jet shifts equatorward. This suggests that it may be limiting to consider only shifts in jet latitude and/or strength when interpreting future distributions of tropospheric constituents, and that more research is needed to quantify future changes in large-scale stationary waves over NH midlatitudes. The mechanisms underlying the stationary wave changes described herein, however, are not well understood and will be investigated in future work.

Acknowledgments. This research was supported by an appointment to the NASA Postdoctoral Program at the Goddard Space Flight Center, administered by Oak Ridge Associated Universities through a contract with NASA. The authors also acknowledge support from ARC Grant DP120100674 (M.H.) and NSF Grants AGS-1403676 (D.W.) and AGS-1402931 (M.H., L.M.P.).

APPENDIX

Air-mass Fractions in Reference (REF) Climate

The climatological mean zonally averaged air-mass fractions for the reference (REF) climate (Fig. A1) facilitate the interpretation of the air-mass fraction changes $\Delta\overline{f}$ discussed in section 4. A closer inspection of the air-mass fractions of oceanic origin (Fig. A2) also demonstrates the correspondence between future changes in low-level convergence and changes in the (re)labeling of air masses near the planetary boundary layer.

REFERENCES

ACIA, 2004: Impacts of a Warming Arctic—Arctic Climate Impact Assessment. Arctic Climate Impact Assessment, Cambridge University Press, 144 pp. [Available online at http://www.acia.uaf.edu/.]

Barnes, E. A., and L. Polvani, 2013: Response of the midlatitude jets, and of their variability, to increased greenhouse gases in the CMIP5 models. *J. Climate*, **26**, 7117–7135, doi:10.1175/JCLI-D-12-00536.1.

Comiso, J. C., 2002: A rapidly declining perennial sea ice cover in the Arctic. *Geophys. Res. Lett.*, **29**, 1956, doi:10.1029/2002GL015650.

Cook, B., and R. Seager, 2013: The response of the North American monsoon to increased greenhouse gas forcing. *J. Geophys. Res. Atmos.*, **118**, 1690–1699, doi:10.1002/jgrd.50111.

Delcambre, S. C., D. J. Lorenz, D. J. Vimont, and J. E. Martin, 2013: Diagnosing Northern Hemisphere jet portrayal in 17 CMIP3 global climate models: Twentieth-century intermodel variability. *J. Climate*, **26**, 4910–4929, doi:10.1175/JCLI-D-12-00337.1.

Frierson, D. M., 2006: Robust increases in midlatitude static stability in simulations of global warming. *Geophys. Res. Lett.*, **33**, L24816, doi:10.1029/2006GL027504.

Hansen, J., and L. Nazarenko, 2004: Soot climate forcing via snow and ice albedos. *Proc. Natl. Acad. Sci. USA*, **101**, 423–428, doi:10.1073/pnas.2237157100.

Holland, M. M., C. M. Bitz, and B. Tremblay, 2006: Future abrupt reductions in the summer Arctic sea ice. *Geophys. Res. Lett.*, **33**, L23503, doi:10.1029/2006GL028024.

Holzer, M., 2009: The path density of interhemispheric surface-to-surface transport. Part II: Transport through the troposphere and stratosphere diagnosed from NCEP data. *J. Atmos. Sci.*, **66**, 2172–2189, doi:10.1175/2009JAS2895.1.

——, and G. J. Boer, 2001: Simulated changes in atmospheric transport climate. *J. Climate*, **14**, 4398–4420, doi:10.1175/1520-0442(2001)014<4398:SCIATC>2.0.CO;2.

Hurrell, J. W., 1995: Decadal trends in the North Atlantic Oscillation: Regional temperatures and precipitation. *Science*, **269**, 676–679, doi:10.1126/science.269.5224.676.

IPCC, 2013: *Climate Change 2013: The Physical Science Basis*. Cambridge University Press, 1535 pp., doi:10.1017/CBO9781107415324.

Koch, D., and J. Hansen, 2005: Distant origins of Arctic black carbon: A Goddard Institute for Space Studies ModelE experiment. *J. Geophys. Res.*, **110**, D04204, doi:10.1029/2004JD005296.

Law, K. S., and A. Stohl, 2007: Arctic air pollution: Origins and impacts. *Science*, **315**, 1537–1540, doi:10.1126/science.1137695.

Lu, J., G. A. Vecchi, and T. Reichler, 2007: Expansion of the Hadley cell under global warming. *Geophys. Res. Lett.*, **34**, L06805, doi:10.1029/2006GL028443.

Lubin, D., and A. M. Vogelmann, 2006: A climatologically significant aerosol longwave indirect effect in the Arctic. *Nature*, **439**, 453–456, doi:10.1038/nature04449.

Miller, R., G. Schmidt, and D. Shindell, 2006: Forced annular variations in the 20th century Intergovernmental Panel on Climate Change Fourth Assessment Report models. *J. Geophys. Res.*, **111**, D18101, doi:10.1029/2005JD006323.

Orbe, C., M. Holzer, L. M. Polvani, and D. Waugh, 2013: Air-mass origin as a diagnostic of tropospheric transport. *J. Geophys. Res. Atmos.*, **118**, 1459–1470, doi:10.1002/jgrd.50133.

——, P. A. Newman, D. W. Waugh, M. Holzer, L. D. Oman, F. Li, and L. M. Polvani, 2015: Airmass origin in the Arctic. Part I: Seasonality. *J. Climate*, **28**, 4997–5014, doi:10.1175/JCLI-D-14-00720.1.

Rothrock, D. A., Y. Yu, and G. A. Maykut, 1999: Thinning of the Arctic sea-ice cover. *Geophys. Res. Lett.*, **26**, 3469–3472, doi:10.1029/1999GL010863.

Senior, C., and J. Mitchell, 1993: Carbon dioxide and climate. The impact of cloud parameterization. *J. Climate*, **6**, 393–418, doi:10.1175/1520-0442(1993)006<0393:CDACTI>2.0.CO;2.

Serreze, M. C., and J. A. Francis, 2006: The Arctic amplification debate. *Climatic Change*, **76**, 241–264, doi:10.1007/s10584-005-9017-y.

——, and Coauthors, 2003: A record minimum Arctic sea ice extent and area in 2002. *Geophys. Res. Lett.*, **30**, 1110, doi:10.1029/2002GL016406.

Shindell, D., G. Faluvegi, A. Lacis, J. Hansen, R. Ruedy, and E. Aguilar, 2006: Role of tropospheric ozone increases in 20th-century climate change. *J. Geophys. Res.*, **111**, D08302, doi:10.1029/2005JD006348.

——, and Coauthors, 2008: A multi-model assessment of pollution transport to the Arctic. *Atmos. Chem. Phys.*, **8**, 5353–5372, doi:10.5194/acp-8-5353-2008.

Simpson, I. R., T. A. Shaw, and R. Seager, 2014: A diagnosis of the seasonally and longitudinally varying midlatitude circulation response to global warming. *J. Atmos. Sci.*, **71**, 2489–2515, doi:10.1175/JAS-D-13-0325.1.

Thompson, D. W., J. M. Wallace, and G. C. Hegerl, 2000: Annular modes in the extratropical circulation. Part II: Trends. *J. Climate*, **13**, 1018–1036, doi:10.1175/1520-0442(2000)013<1018:AMITEC>2.0.CO;2.

Trenberth, K. E., and J. W. Hurrell, 1994: Decadal atmosphere–ocean variations in the Pacific. *Climate Dyn.*, **9**, 303–319, doi:10.1007/BF00204745.

Wadhams, P., and N. R. Davis, 2000: Further evidence of ice thinning in the Arctic Ocean. *Geophys. Res. Lett.*, **27**, 3973–3975, doi:10.1029/2000GL011802.

Wetherald, R., and S. Manabe, 1988: Cloud feedback processes in a general circulation model. *J. Atmos. Sci.*, **45**, 1397–1416, doi:10.1175/1520-0469(1988)045<1397:CFPIAG>2.0.CO;2.

Woollings, T., and M. Blackburn, 2012: The North Atlantic jet stream under climate change and its relation to the NAO and EA patterns. *J. Climate*, **25**, 886–902, doi:10.1175/JCLI-D-11-00087.1.

Wu, Y., M. Ting, R. Seager, H.-P. Huang, and M. A. Cane, 2011: Changes in storm tracks and energy transports in a warmer climate simulated by the GFDL CM2.1 model. *Climate Dyn.*, **37**, 53–72, doi:10.1007/s00382-010-0776-4.

Yin, J. H., 2005: A consistent poleward shift of the storm tracks in simulations of 21st century climate. *Geophys. Res. Lett.*, **32**, L18701, doi:10.1029/2005GL023684.

Zelinka, M. D., S. A. Klein, K. E. Taylor, T. Andrews, M. J. Webb, J. M. Gregory, and P. M. Forster, 2013: Contributions of different cloud types to feedbacks and rapid adjustments in CMIP5. *J. Climate*, **26**, 5007–5027, doi:10.1175/JCLI-D-12-00555.1.

Zhang, Y., J. M. Wallace, and D. S. Battisti, 1997: ENSO-like interdecadal variability: 1900–93. *J. Climate*, **10**, 1004–1020, doi:10.1175/1520-0442(1997)010<1004:ELIV>2.0.CO;2.

Zhou, S., A. J. Miller, J. Wang, and J. K. Angell, 2001: Trends of NAO and AO and their associations with stratospheric processes. *Geophys. Res. Lett.*, **28**, 4107–4110, doi:10.1029/2001GL013660.